Journal of Materials Research and Technology 36 (2025) 627–640

Contents lists available at ScienceDirect

Journal of Materials Research and Technology

journal homepage: www.elsevier.com/locate/jmrt

Mechanical properties, corrosion resistance and microstructural analysis of recycled aggregate concrete made with ceramic wall waste and ultrafine ceria

Ansam Ali Hashim [a,b], Rana Anaee [b], Mohammed Salah Nasr [c,*], Ali Shubbar [d], Turki S. Alahmari [e]

[a] Technical Institute of Babylon, Al-Furat Al-Awsat Technical University, Iraq
[b] Department of Materials Engineering, University of Technology, Baghdad, Iraq
[c] College of Engineering, University of Babylon, Babylon, Iraq
[d] School of Civil Engineering and Built Environment, Liverpool John Moores University, Liverpool, L3 3AF, UK
[e] Department of Civil Engineering, Faculty of Engineering, University of Tabuk, P.O. Box 741, Tabuk, 71491, Saudi Arabia

ARTICLE INFO

Handling editor: M Meyers

Keywords:
Ultrafine cerium oxide
Recycled aggregate concrete
Corrosion resistance
Microstructure analysis
Mechanical characteristics

ABSTRACT

This study examines how incorporating ultrafine cerium dioxide particles (UFCe) into recycled coarse aggregate concrete affects its physical, mechanical, and long-term properties. No analogous research exists about the impact of ultrafine cerium dioxide particles on various characteristics of concrete containing recycled aggregates (RCA). UFCe was employed, and its mean particle size was 350 nm in different doses (0.0, 0.5, 1.0, and 1.5 % by cement weight) to explore its effect on the properties of concrete containing 25 % coarse aggregates (RCA) prepared from ceramic wall waste. The setting time, slump flow, porosity, water absorption, compressive and tensile strengths, electrical resistance, chloride penetration resistance, corrosion resistance, and microstructure analysis were investigated. The findings indicated that UFCe significantly enhanced the compressive and tensile strength while decreasing water absorption and pore ratio comparison to the control mixture after 90 days of curing. Moreover, all mixtures displayed significantly lower chloride penetration depth and corrosion rate than the reference mixture. The inclusion of UFCe additionally improved the microstructure due to the enhancement of the ultrafine particle hydration process. On the other hand, the optimum improvement of mechanical strength, durability properties, and microstructure was recorded at a UFCe replacement rate of 0.5 %. For example, the compressive and tensile strengths increased by 33 % and 9 %, respectively, while the total water absorption and migration coefficient were reduced by 42 % and 67 % at 90 days, respectively, compared with the reference sample.

1. Introduction

Concrete has emerged as a widely utilized building material due to its numerous advantages, including the accessibility of its components, exceptional durability, little maintenance expenses, low-skilled labor requirements, and significant fire resistance. It is cited as the 2nd most utilized material, with around three tons consumed per individual globally [1–3]. Concrete significantly affects the environment due to its constituents [4,5]. Cement manufacture significantly contributes to carbon dioxide emissions, with the generation of one ton of cement emitting 709 kg of CO2 [6,7] during the production process. The proportion of aggregates utilized in concrete is a significant issue since they account for approximately 80 %–85 % of its overall volume, depleting natural resources [8,9]. As a result, other sources—such as industrial waste from various sources—may be crucial to the efficient manufacture of concrete. In addition to lowering CO2 emissions and conserving landfill space, using recycled materials like aggregates in concrete manufacturing also preserves natural resources and lowers the cost of new concrete [10]. Furthermore, incorporating waste materials into concrete production might help reduce the substantial amount of waste generated by the industry [11–14]. Among these wastes are ceramic and tile waste, which are the most extensively utilized

* Corresponding author.
E-mail addresses: ansamly2@atu.edu.iq (A.A. Hashim), dr.rana_afif@yahoo.com (R. Anaee), eng511.mohammed.nasr@uobabylon.edu.iq, msn_alamar@yahoo.com (M.S. Nasr), a.a.shubbar@ljmu.ac.uk (A. Shubbar), talahmari@ut.edu.sa (T.S. Alahmari).

https://doi.org/10.1016/j.jmrt.2025.03.154
Received 14 January 2025; Received in revised form 13 March 2025; Accepted 17 March 2025
Available online 18 March 2025

construction materials globally [15]. The waste produced during manufacturing includes ceramic and tile waste that results from production defects. During the last stage of manufacture, 3–7 % of the ceramic and tile produced worldwide is discarded as waste [16]. Recently, the use of waste, especially industrial commodity components [17], has increased to create environmentally friendly concrete and enhance its quality. Furthermore, much research has been conducted utilizing ceramic waste as a viable substitute for natural coarse and fine aggregates in concrete. According to several studies, cement-based products (concrete or mortar) are stronger when ceramic-based materials are used in place of coarse and/or fine particles.

At all levels of replacing natural aggregates with ceramic electrical insulation waste, Gharibi et al. [18] found that the compressive strength rose. The water absorption decreased when the crushed ceramic electrical insulation waste was replaced separately with natural sand and gravel at 25, 50, 75, and 100 %, as well as when the coarse and fine insulation waste was replaced together at 50 and 100 %. Suzuki et al. [19] found an improvement in physical properties without any decrease in compressive strength at early or late ages when porous ceramic aggregates (PCCA) made from recycled waste were used instead of natural aggregates at 10, 20, 30, and 40 %. González et al. [20] found that concrete produced using ceramic sanitary blocks by completely replacing conventional aggregates (gravel) in structural concrete had mechanical properties equivalent to those prepared with conventional aggregates. Torkittikul and Chaipanich [21] demonstrated that concrete manufactured using CWA as a sand replacement at 0 %, 10 %, 20 %, 30 %, 40 %, 50 %, and 100 % has low workability with increasing the amount of ceramic waste and that its compressive strength falls as the amount of ceramic waste increases, peaks at 50 %, and subsequently decreases when ceramic waste content exceeds 50 %. The study carried out by Xu et al. [22] indicates that the highest compressive strength was obtained by substituting 20 % of the natural coarse aggregate with ceramic wall aggregate. Nonetheless, other investigations have demonstrated a reduction in strength with the augmented use of recycled ceramics. for example, Compressive strength diminished by 3 %, 5 %, 9 %, 28 %, 34 %, and 44 % at 100 % replacement [22–27], whereas it reduced by 24 % at both 30 % and 50 % replacement [28,29]. The variation in outcomes associated with ceramic aggregate arises from the diverse origins of ceramic waste, such as sanitary ceramics, floors, ceilings, insulators, kitchen utensils, electrical insulators, bricks, etc. [30]. When various kinds of ceramic aggregate are employed, concrete's porosity and water absorption improve while its density decreases. This is because ceramic aggregate absorbs more water than natural aggregates. The ceramic aggregate concrete's chloride penetration resistance was inadequate due to its heightened porosity. As a result, ceramic aggregate concrete has subpar permeability properties relative to traditional concrete. Consequently, the steel immersed in RAC experiences corrosion, resulting in a loss of its cross-sectional area and a significant decrease in the lifespan of the reinforced structure, potentially culminating in its failure [31]. Different pre-treatment methods have been employed to augment RAC's robustness and longevity and address the constraints of RCA. These methods consist of nanomaterial modification [32], accelerated carbonation technique [33], and microbial carbonate precipitation [34]. Concrete's strength and durability may be increased with the right nanoparticle. They do this by covering the aggregates' surface, decreasing the concrete's permeability, filling the micropores to lessen porosity, accelerating the cement's hydration reaction, and strengthening the bonds that bind the aggregates to the cement paste [35,36]. Nanotechnology has great promise for enhancing concrete's performance and producing novel, eco-friendly, advanced cement composites with unique mechanical, thermal, and electrical properties [37]. Cerium oxide (CeO_2) is a rare-earth metal oxide; its hydrolysis byproduct is a white precipitate [38,39]. Cerium oxide is currently used as an additive in the glass industry, especially for grinding flat glass, as shown by numerous studies [40,41]. In the field of optoelectronics, cerium oxide has anti-ultraviolet properties [42,43]. It has also been used to coat refractory bricks to give them resistance to radiant heat [44]. The beneficial effects of cerium oxide in corrosion-resistant coatings have been the subject of numerous investigations [45–49].

Table 1
Chemical analysis and physical attributes of PC and UFC.

Chemical analysis(wt.%)	PC	UFCe
CeO2	–	94.65
SiO2	21.84	0.4
Al2O3	4.72	0.005
CaO	61.41	0.321
Fe2O3	3.60	0.620
MgO	2.97	0.190
K2O	0.65	–
Na2O	0.29	–
SO3	2.26	–
TiO2	1.69	0.187
Physical characteristics		
D50 (μm)	0.350	10.98
Specific gravity	3.15	6.32

Table 2
Physical characteristics of RCA, NCA, and RCA.

Items	RCA	NFA	NCA
Fineness Modulus	6.9	2.91	6.2
Unit Weight (kg/m^3)	1083	1660	1640
Water Absorption (%)	16	0.93	0.47
Specific Gravity	2.46	2.65	2.58

Nevertheless, the effects of cerium oxide on cementitious materials have only been the subject of a small number of research [50,51]. No previous work examined the impact of ultrafine cerium oxide (as a substitute for cement) on the characteristics of concrete formulated with coarse aggregates derived from wall ceramic waste. Furthermore, very limited studies (or even no one) investigated the corrosion resistance of recycled aggregate concrete created using ultrafine CeO_2. Therefore, the current study's purpose is to examine how UFCe, which has an average particle size of 350 nm, affects the physical and mechanical features of concrete comprising 25 % coarse aggregates derived from wall ceramic waste (RCA). Cement was substituted with different concentrations of UFCe (0.5, 1.0, and 1.5 wt%). The investigated properties were setting time, slump flow, porosity, water absorption, compressive, tensile strength, electrical resistance, and chloride penetration resistance. The corrosion resistance of RA-UFCe concrete at 5 % NaCl was also studied. Finally, the microstructural properties were carefully investigated.

2. Materials and methods

2.1. Materials used

This research utilized "Type I" ordinary Portland cement (PC) made by ALMAS Cement Company Limited in Iraq, as categorized by ASTM (ASTM C 150, 2017) [52]. Ultra-fine cerium dioxide was produced by grinding micronized cerium dioxide powder with a 20.99 μm mean particle size and a purity of 94.65 % in a nano ball mill for 2 h. The fineness of cement and ultrafine cerium dioxide particles was verified using a laser particle analyser (Malvern MS3000) where D50 = 10.96 μm and 0.350 μm, respectively; see Fig. 2. Table 1 displays the outcomes of the X-ray fluorescence (XRF) chemical analysis of PC and UFCe. It also shows the physical characteristics of PC and UFCe. As shown in Fig. 2, locally available broken wall ceramics were crushed with a hammer to obtain coarse ceramic aggregate (RCA) with a maximum particle size of 19 mm. River sand and crushed gravel are examples of natural fine aggregate (NFA) and natural coarse aggregate (NCA), with maximum particle sizes of 4.75 and 19 mm, respectively. The crushed gravel's physical attributes complied with Iraqi standards (IQS No.45) [53]. The

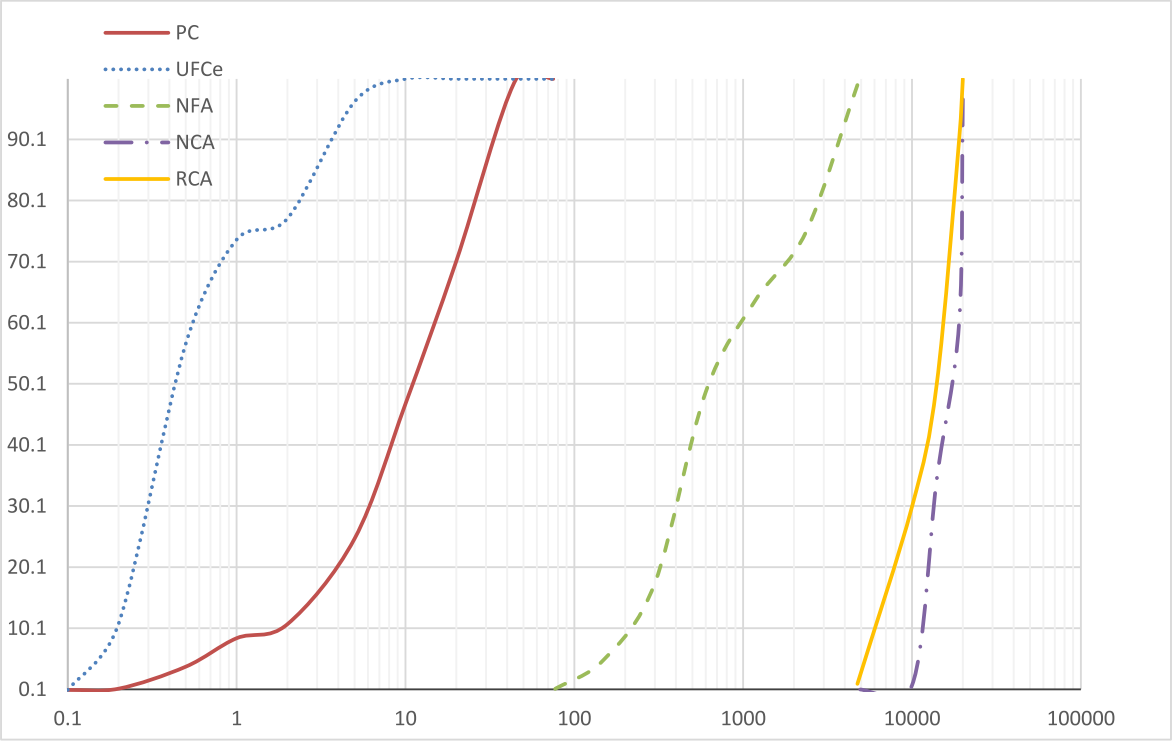

Fig. 1. Patterns of particle sizes for UFC, PC, RCA, NFA, and NCA.

Fig. 2. The procedure for generating ceramic coarse aggregate from wall ceramic waste.

physical properties of natural coarse aggregate (NCA), natural fine aggregate (NFA), and coarse ceramic aggregate (RCA) are compiled in Table 2. The particle size distribution of PC, UFCe, RCA, NCA, and NFA is presented in Fig. 1. Commercially accessible Hyperplastic PC200, a high-range water reducer (superplasticizer) that meets ASTM C494 Type F criteria [54]was employed. Water with a pH of 7.5 was employed to produce all RAC mixes. In addition, four iron bars 10 mm in diameter and 150 mm in length were utilized for the corrosion test.

2.2. Mixing proportions

This study used 25 % of ceramic coarse aggregate to replace natural coarse aggregate. 0 %.0.5 %, 1 %, and 1.5 % were utilized as a substitute for PC. To achieve sufficient workability and a target mean strength of 30 MPa, a super-plasticizer admixture amounting to 1.6 % of the cementitious materials was used in all concrete mixes, with a constant

Table 3
Mixing proportion of concrete (kg/m^3).

Ingredients	RCA-UFCe0	RCA-UFCe0.5	RCA-UFCe1	RCA-UFCe1.5
PC	375	373.125	371.25	369.375
UFCe	0	1.875	3.75	5.625
RCA	250	250	250	250
NFA	750	750	750	750
NCA	750	750	750	750
Water	0.5	0.5	0.5	0.5
Superplasticizer	1.6	1.6	1.6	1.6

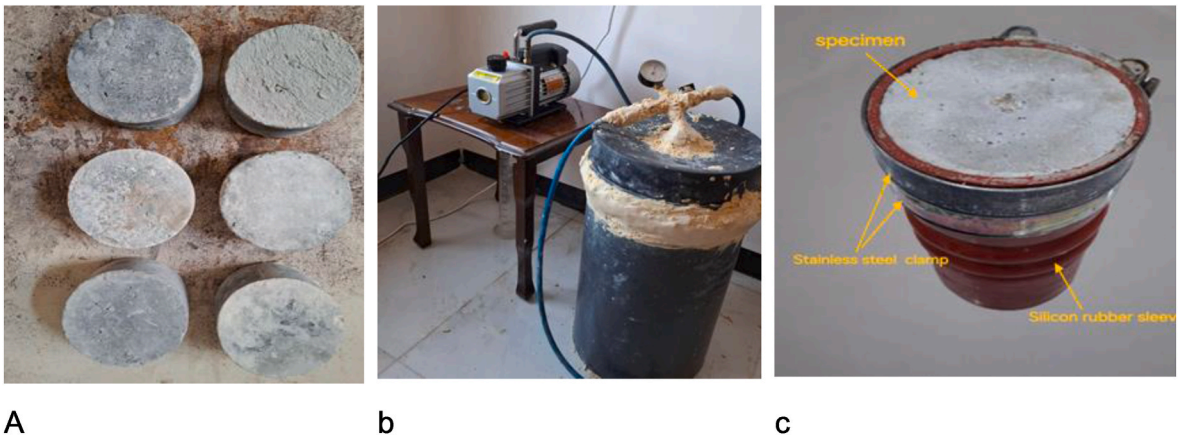

Fig. 3. (a) Samples of concrete for chloride migration, (b) Vacuum container, (c) Cylinder rubber tube.

water-to-binder ratio of 0.5. The mixing ratios for every RCA concrete mixture are displayed in Table 3.

2.3. Setting up specimens

The samples were prepared by mixing the ceramic aggregates, coarse aggregates, and fine aggregates in a mixer for 1–2 min. This ensures that all types of aggregates are evenly distributed. The aggregate mixture is then mixed for another minute with half the amount of mixing water added. This step aims to hydrate the aggregates. After this step, the cement is poured into the mixer, the remaining water is added and mixed with the ultra-fine cerium oxide after mixing it with water using the mixer for a minute. This step aims to ensure that there are no clumps of ultra-fine cerium oxide. Then, the plasticizer is added to this mixture and poured into the mixer. After adding all the ingredients, the mixer is turned on for a minute to ensure homogeneous distribution of all components of the concrete mixture. After the mixing process was complete, concrete specimens were formed in standard, sealed molds with oiled interior surfaces to prevent the concrete from sticking together once it had hardened. The concrete mix was poured also into cubic, cylindrical, prismatic, and disc molds. After the mix was placed in the molds, an electric vibration mechanism compacted the concrete samples, preventing the formation of air pockets and ensuring compaction. The molds were removed after 20–24 h of pouring. Each RCA-UFCe concrete specimen was submerged in water reservoirs at ambient temperature for durations of 28 days and 90 days, as dictated by the requirements of each respective test.

2.4. Program of testing

This research involved a number of experiments, which are described in the following sections.

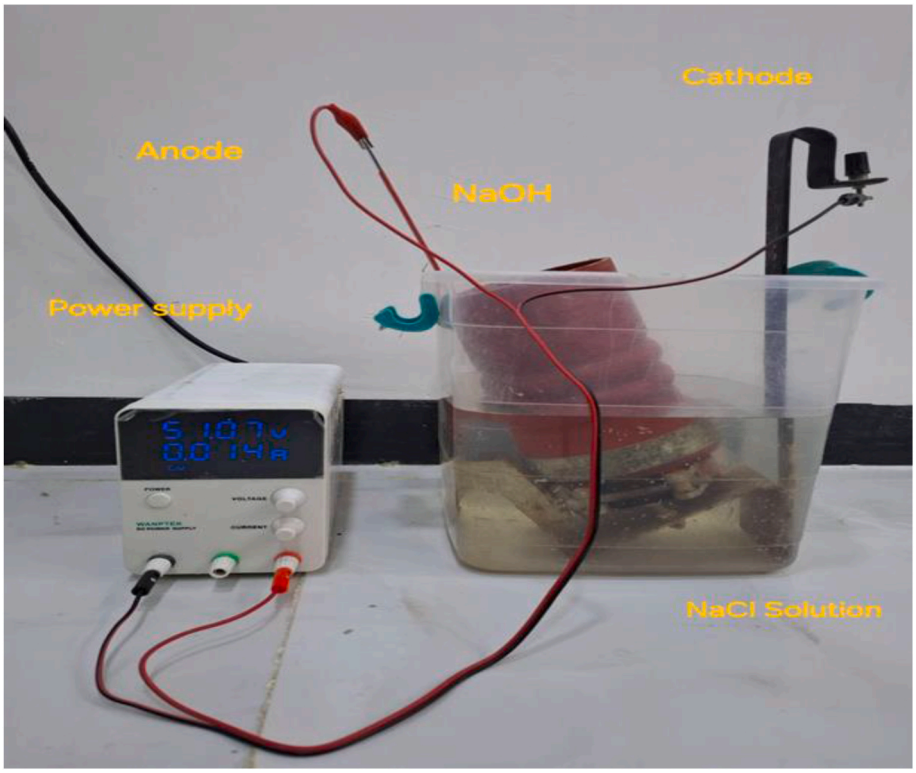

Fig. 4. Rapid Chloride migration test setup.

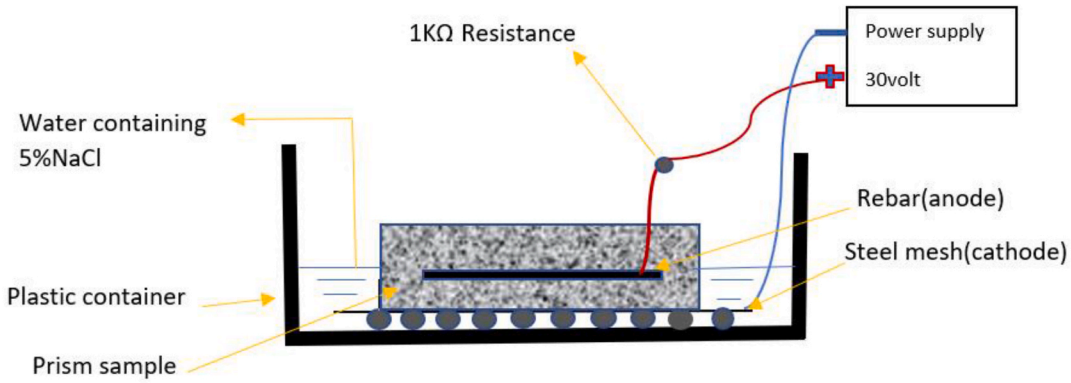

Fig. 5. The impressed current accelerated corrosion test setup and components.

2.4.1. Fresh tests (workability and setting times)

All RCA -UFCe concrete mixtures are tested for workability using the slump test in accordance with the ASTM-C 143 standard [55]. A Vicat instrument was used to perform a setting time test according to ASTM C191-82 [56].

2.4.2. Hardened tests

2.4.2.1. Compressive strength. The examination is performed per the guidelines outlined in BS 1881-Part 116 [57]. To examine the change in compressive strength over time, a set of twenty-four 100 mm concrete cubes was made in different concrete mixtures. The ages being examined are 28 and 90 days. For every mixture, three cubes are generated at the specified age.

2.4.2.2. Tensile strength. Tensile strength tests were conducted on cylindrical specimens that were 100 mm in diameter and 200 mm in height at 28 and 90 days of age using ASTM-C496 standard procedures [58].

2.4.2.3. Bulk density. The density test was carried out on the same cubes whose compressive strength was to be measured, by accurately measuring the weight and volume of the cubes while they were in a saturated, dry state on the surface. The apparent density was determined by dividing each cube's weight by its volume. For every mixture, three cubes were examined and the mean value was adopted to represent the result.

2.4.2.4. Total water absorption and permeable voids. These tests were conducted using 100-mm cubes each, and the permeability and total water absorption tests were carried out following ASTM C642 guidelines [59].

2.4.2.5. Bulk electrical resistivity (ER). According to ASTM C1876-19 [60], the total resistivity was measured in Ω/cm using the two-metal plate technique on saturated cubic specimens of dimensions 100 mm using a DER EE LCR meter, made in Taiwan, for measuring impedance at a frequency of 1 KHz [61].

2.4.2.6. Test for chloride migration. As seen in Fig. 3 (a), cylindrical specimens of 100 mm in diameter and 50 mm in height were cast and utilized for the Nordtest technique's quick chloride migration test [62]. For each mixture, three concrete samples were cast, and they were cured in water for 28 and 90 days. After that, the specimens were put in a vacuum chamber (Fig. 3 (b)). After exposing the specimen's two end sides, the vacuum vessel's internal absolute pressure was increased to between 1 and 5 kPa in a matter of minutes, and the vacuum was kept there for 3 h. The vacuum pump operated continuously to fill the vacuum vessel with a saturated solution of Ca (OH)2, utilizing the pressure differential between the vessel and the container carrying Ca (OH)2. This immersed all specimens and prevented the leakage of Ca (OH)2. After an hour of maintaining the vacuum, the air was allowed to return to the container. The Nordtest method involved immersing the specimens in the Ca(OH)2 solution for 18 ± 2 h and applying an electric circuit on a solution of sodium hydroxide and sodium chloride to speed up the chloride penetration. Each specimen was set inside a cylindrical rubber tube secured with two clamps, as shown in Fig. 3(c). In NaOH and NaCl solutions, electrodes represent the anode and cathode, respectively, the sample's top surface was exposed to a 300 g/mL sodium hydroxide (0.3 N NaOH) solution. Fig. 4 displays the setup for the fast chloride migration test. After exposure, a 0.1 N silver nitrate (AgNO3) solution was applied to the sample's fractured portion and measured the chloride penetration (xd) that results from the interaction between Cl and Ag+. The depth of chloride ions (xd) was determined. The unsteady migration diffusion coefficient (Dnssm) may be calculated using the depth of chloride penetration in the short cylinder, as indicated by Eq. (3).

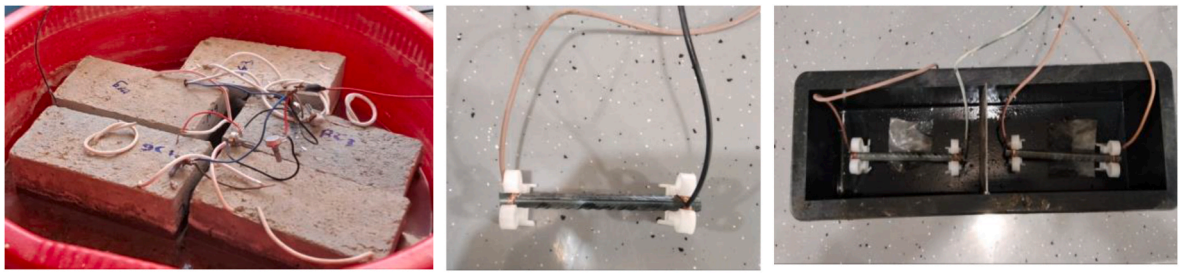

Fig. 6. (a) Prismatic specimens with dimensions of 100*100*200 mm^3(b) Steel rebar secured with copper wires and (c) Plastic prismatic mold with fastened rebar.

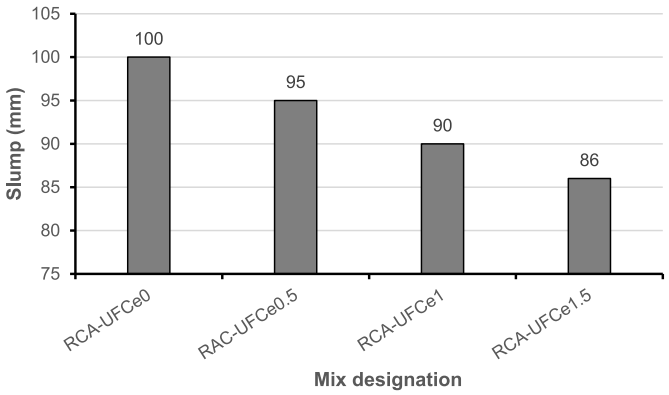

Fig. 7. RCA concrete mix slump value with and without UFCe.

$$Dnssm = \frac{0.0239(273+T)lt}{(Uv-2)t}\left(xd - 0.0238\left(\sqrt{\frac{(273+T)lt\,xd}{Uv-2}}\right)\right) \quad (3)$$

U represents the absolute voltage magnitude. T is the mean of the anode's initial and final solution temperatures. L denotes the sample's thickness, which in this investigation is 50 mm, whereas t represents power-on duration (24 h in this investigation).

2.4.2.7. Accelerated corrosion by impressed current technique. The corrosion of steel is a somewhat gradual process. Corrosion start requires a much-extended period caused by the alkaline properties of concrete, even when subjected to harsh corrosive environments. The extended durations required for recreating reinforcement corrosion in laboratories have led to the creation of rapid corrosion testing procedures. The impressed current approach is recognized as an efficient and rapid method among many accelerated corrosion test methods, significantly shortening the corrosion beginning period for de-passivation from years to days [63]. This approach involves applying a constant direct current (DC) to the steel embedded within the concrete to induce corrosion. The current is impressed from the electrode to the reinforcement through concrete immersed in an electrolyte (sodium chloride solution) [64]. The configuration for the impressed current accelerated corrosion test is depicted in Fig. 5. In this study, prismatic specimens with dimensions of 100*100*200 mm3(see Fig. 6 (a) and steel bars with length of 15 cm and diameter of 10 mm were used, and their weight was measured before subjecting them to the accelerated corrosion process to use this weight to calculate the weight loss resulting from corrosion. The steel bars were tied with copper wires before inserting them into the prismatic mold with dimensions of 2 cm cover as seen in Fig. 6(b) and (c). In the concrete casting process, the bars were fixed within the mold, after which the concrete was poured and subjected to a mechanical vibrator to achieve enough compaction around the reinforcing steel, so establishing a robust connection between the concrete and the reinforcing steel bar. Following 24 h, the solidified samples were extracted from the molds and subjected to tap water treatment for 28 days. Upon completion of the treatment period (28 days), the samples were removed from the water and allowed to dry for 24 h, after which the samples were placed in a solution containing 5 % sodium chloride, and a steel mesh was placed under the sample and connected with wires to a continuous power source representing the cathode pole. As for the electrical wires in the sample, they were connected to a variable resistance (1 kilo-ohm) and attached as the anode pole to the power supply. Then the current was applied while maintaining a constant voltage as shown in. Then equation (4) was used to determine the applied current and needed time based on applying a current density of 0.3 mA/cm2 to achieve a 10 % corrosion rate in the steel rod following Faraday's law [65]:

$$t=(m*z*F)/(M*I) \quad (4)$$

Table 4
Cement pastes' initial and final setting times, both with and without UFCe.

Proportion of Cement Substitution	Initial Time of Setting (min)	Final Time of Setting (min)
UFCe0	120	170
UFCe0.5	114	165
UFCe1	112	160
UFCe1.5	110	156

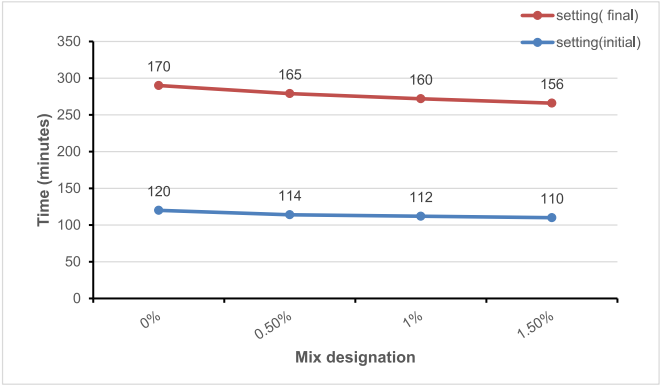

Fig. 8. RCA concrete mix initial and final setting value with and without UFCe.

where: Z = valence (2), M = mass loss from corrosion (gm), t = time (second), M = atomic weight of metal (55.85), I = imposed current (A), and F=Faraday's constant (96480 A s) Steel rebar density is 7.85 g/cm3, and its mass is equal to 7.85x π x 0.5 × 2 x 15 = 92.48 gm.

For 26 days, the current delivered to each sample was 14.137 mA, but the temperature and solution height—that is, 25 °C and 50 mm below the sample's top surface, respectively—stayed constant.

2.4.2.8. Microstructural analysis. A scanning electron microscope (SEM) was utilized to examine the microstructure. A small sample of concrete, measuring about 5 by 5 mm, was taken out of each specimen for this analysis. The sample was desiccated in an oven maintained at 105° Celsius for 24 h. After that, diamond paste was used to clean its surface. After applying a copper light coating to the specimen to get an electrical charge, it was placed on an SEM stem.

3. Results and discussion

3.1. Slump

As shown in Fig. 7, the slump was measured for the partly UFCe replacement mixtures and the control concrete mix as soon as the water was added and combined. The RCA-UFCe0 concrete mix's slump value was discovered to be 100 mm. After that, when the replacement started, increasing the dosage of UFCe from 0.5 % to 1.5 %, the slump of UFCe-modified RCA concrete was reduced. This can be explained by the large surface area of UFCe particles and increased free water absorption [66, 67]. The RCA-UFCe0 mix recorded the highest slump value of 100 mm. While RCA-AFCe1.5 recorded the lowest slump value, which is 85 mm.

3.2. Initial and final setting time

Table 4 and Fig. 8 Provide the initial (IS) and final (FS) setup timeframe outcomes for cement pastes with 0 %, 0.5 %, 1 %, and 1.5 % UFCe.

The IS and FS varied from 120 to 110 min and 170 to 156 min, respectively. The cement paste, including 100 % cement (control mix), exhibited the highest values for both IS and FS. Replacing PC with UFCe shortened the setting time as the pastes started to lose their elasticity, and the maximum variation was recorded in pastes comprising 1.5 wt%

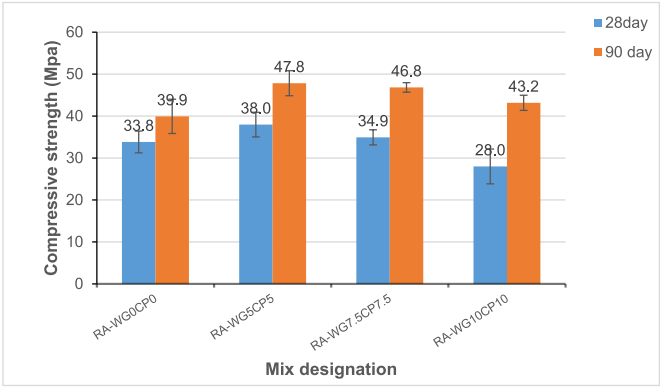

Fig. 9. RCA concrete mix compressive strength value with and without UFCe at 28 and 90 days.

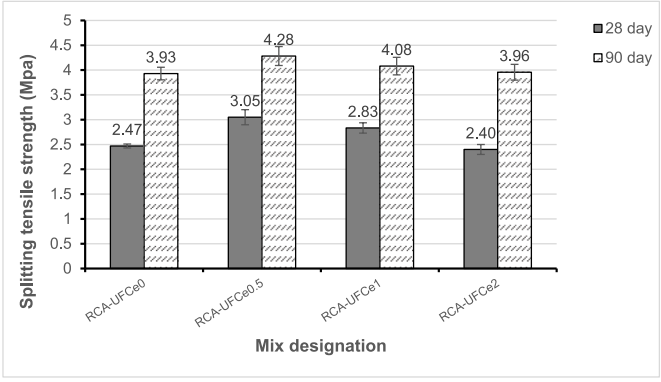

Fig. 10. RCA concrete mix tensile strength value with and without UFCe at 28 and 90 days.

UFCe (110 min, 10 min faster than the reference mix). According to the effect of supplementary cementing materials BFS and FA on hydration, ultra-fine CeO2 particles accelerate the hydration and setting process [68,69]. Since the cerium absorbs water (54 % by volume), it eliminates surplus free water, which lowers the w/b ratio and causes the setting time to decrease as the UFCe concentration increases [67].

3.3. Compressive strength

Fig. 9 displays the compressive strength test findings conducted at 28 and 90 days of age for the control mixture and those with UFCe. Each reported number included the mean of three measurements. According to the results, the compressive strength rose at 28 days of age when ultrafine cerium oxide was added up to a 1 % replacement ratio. The concrete mixes RCA-UFCe0.5, and RCA-UFCe1 had respective compressive strengths of 45 and 41 MPa, which were 33 % and 21 % higher than those of the control mix, RCA-UFCe0. The RCA-UFCe1.5 mix's compressive strength, 33.17 MPa, is comparable to the reference mix. Because the UFCe particles were smaller than the cement particles, they had a filling effect; by filling the gaps between the cement paste and the aggregate, the UFCe grains could increase the microstructure's density and raise its compressive strength [70]. However, at 90 days, all RCA-UFCe mixtures containing ultrafine cerium oxide showed satisfactory compressive strength results. RCA concrete containing (0.5 %, 1 %, and 1.5 %) UFCe obtained compressive strengths of 52.93, 45.83, and 42.33 MPa at the end of 90 days, which is about 32.6 %, 14.8 %, and 6 % higher than 39.93 MPa recorded for RCA-UFCe0 at the same age. In comparison to the strength values at 28 days, the compressive strengths of the RCA-UFCe mixes were improved by longer curing times, according to the recorded data. The improvement of the ultrafine particle

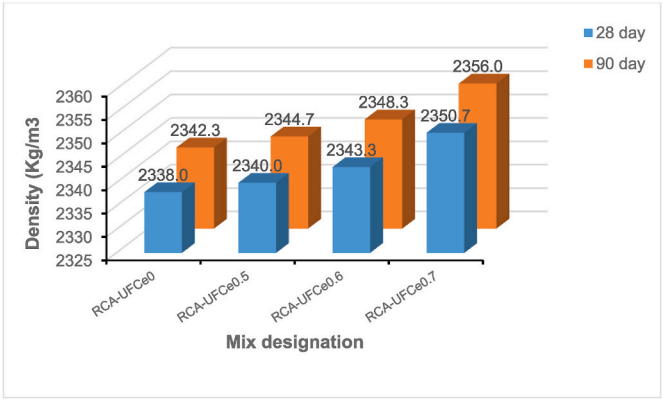

Fig. 11. RCA concrete mix bulk density value with and without UFCe at 28 and 90 days.

hydration process, which results in the formation phases C–Ce–H, C–Ce-AH, and C–Ce-A-S-H as well as C–S–H, C-A-H, and C-A-S-H-gel phases from the pozzolanic action of ultrafine cerium oxide with free portlandite, which is released by hydration of PC, is the cause of the increase in compressive strength of the RCA-UFCe concrete specimen containing ultrafine CeO2 particles with age [51].

3.4. Splitting tensile strength

Fig. 10 shows the cylindrical (10 × 20) mm tensile strength test results at 28 and 90 days of age. The mean of three measurements was taken to calculate the tensile strength results. A similar pattern to that of compressive strength was observed in the tensile strength of RCA-UFCe mixtures containing UFCe. The split tensile strength of RCA-UFCe mixtures was found to increase with increasing curing ages. Compared with the RCA-UFCe0 blend, the split tensile strength of all UFCe-containing blends increased at longer curing times (90 days). For example, the tensile strength of RCA-UFCe0.5, RCA-UFCe1, and RCA-UFCe1.5 blends was found to be 4.28, 4.08, and 3.96 MPa, which were about 9 %, 4 %, and 1 % higher than the tensile strength of RCA-UFCe0 blends at the same curing time. The increase in tensile strength with increasing curing times indicates the development of hydration products and the production of increasing amounts of C–S–H, C-A-H, and C-A-S-H-gel as the main source of strength [51,71]. The precipitation and accumulation of these hydration products in the empty and unoccupied pores results in a more compact and uniformly hardened cementitious body [51].

3.5. Bulk density

Mortar or concrete's bulk density is defined by a number of factors, such as the amount and density of aggregate, the amount of water and cement, and the presence or absence of trapped or entrained air spaces [72]. Fig. 11 shows how the density of RCA concrete mixtures is impacted by the concrete's age and the UFCe replacement ratio. The results revealed two patterns. In the first place, the density increased with age, at 28 and 90 days, the density of RCA-UFCe0, RCA-UFCe0.5, RCA-UFCe1, and RCA-UFCe1.5 concrete mixes were (2338,2340, 2343and 2350) and (2342,2345,2348and 2356) g/cm3 respectively. The continuous progress of the hydration of cement phases, along with the enhancing effect of UFCe, has significantly boosted hydration and the pozzolanic action. This process leads to the formation of additional cementitious materials in the hydrated gel products of C–Ce–H, C–Ce-AH, and C–Ce-A-S-H. These hydration products serve as binding cores among the cementitious grains that precipitate within the open pores of the matrix. Second, an increase in the density as a function of UFCe replacement, by increasing the content of ultra-fine cerium oxide the bulk density increased, where the highest density value was

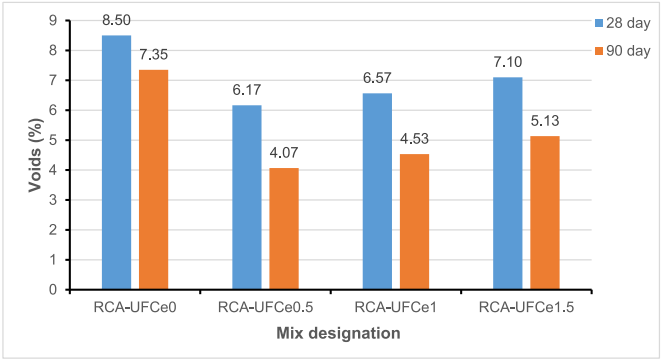

Fig. 12. RCA concrete mix percentage of permeable void value with and without UFCe at 28 and 90 days.

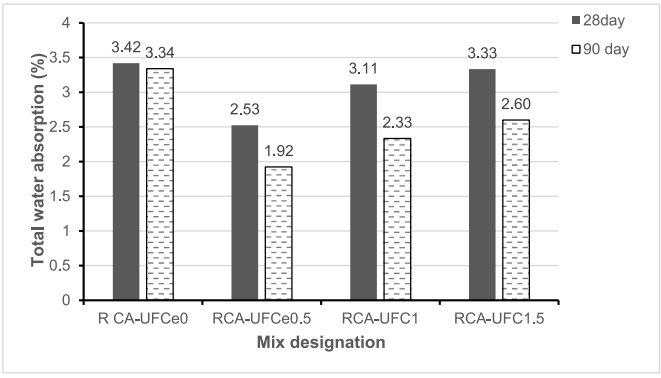

Fig. .13. RCA concrete mix total water absorption value with and without UFCe at 28 and 90 days.

recorded for the mixture containing 1.5 % UFCe. This is because the specific gravity of the ultra-fine CeO2 particles is 6.32, which is roughly twice that of cement. Moreover, by filling in the spaces, the tiny UFCe particles might have made RCA concrete more compatible and produced a denser microstructure [73].

3.6. Percentage of permeable voids

The porosity of hardened concrete is considered a crucial factor in its durability. Improving concrete's durability and longevity under extreme conditions is as simple as reducing the number of empty spaces inside the material. Because of the basic inverse link between porosity and the strength of solid materials, reducing porosity has a favorable influence on concrete's compressive and flexural strengths. One common way to measure the void content of concrete and thus its durability is the water absorption test [74]. The percentage of permeable voids at 28 and 90 days of age is shown in Fig. 12. The findings demonstrated that the percentage of permeable voids of all RCA concrete mixtures containing UFCe was less than that of the RCA-UFCe0 mix. Moreover, the rate of permeable voids was decreased with ongoing hydration. The RCA-UFCe0.5 mix showed a lower rate of permeable pores and higher compressive strength than other RCA-UFCe mixes since concrete's porosity and compressive strength are strongly correlated [75]. Its pore content was 6.17 % and 4.07 % at 28 and 90 days, respectively, 27.5 % and 36 % lower than the RCA-UFCe0(reference mix). The decrease in porosity is the result of continuous hydration. UFCe forms calcium silicate (C–S–H) and hydrogel products of calcium silicate, cerium, aluminate, and silicate by reacting with free portlandite produced by cement hydration. The development of these hydrated gel products reduced the number of big open pores and increased the filling capacity, creating a denser and less porous microstructure [76].

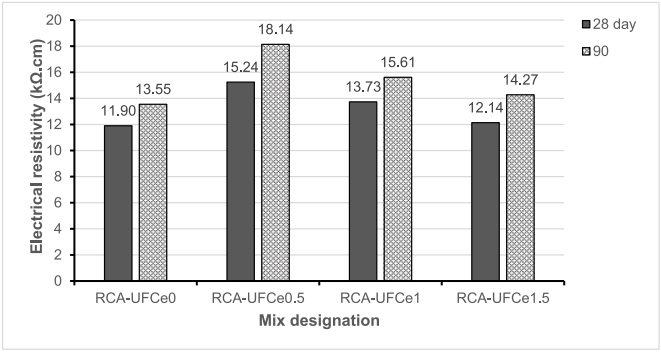

Fig. 14. RCA concrete mix electrical resistivity value with and without UFCe at 28 and 90 days.

3.7. Total water absorption (TW)

The water absorption test is efficient for evaluating concrete's capillary suction and durability under harsh conditions. The movement of water within concrete greatly influences its durability [77]. Three main factors influence water absorption: the interfacial transition zone (ITZ), the chemical makeup of the porous matrix, and the arrangement of pores. These factors are essential throughout the early phases of formation [78]. Fig. 13 displays the water absorption results following 28 and 90 days. The outcomes showed that all mixes, including UFCe, had lower total absorption values at 28 and 90 days of age than the control specimen. The total water absorption of RCA-UFCe mixtures, including UFCe, showed a similar pattern to that of the percentage of permeable voids. The (TW) of the RCA-UFCe mixes diminished with prolonged curing durations. The incorporation of 0.5 % UFCe (RCA-UFCe0.5 mix) yielded a reduced water absorption value compared to the RCA concrete mix containing 1.0 % and 1.50 % by mass of CeO2 ultra-fine particles. This result was ascribed to the incorporation of ultrafine particles, which facilitated the segmentation of large holes and improved nucleation sites for the precipitation of hydration products in the cement paste, resulting in pore refinement and improved dispersion of hydration products [79] Furthermore, the gradual hydration process results in the development of hydrated compounds. Such hydrated compounds accumulate in the open pores present [80]. At 28 days the water absorption of RCA-UFCe0.5, RCA-UFCe1, and RCA-UFCe1.5 mixes made with 0.5 %, 1 %, and 1.5 % UFCe in comparison to the control mixture decreased by (26 %, 9 %, and 3 %), respectively, and at 90 days decreased by 42 %, 30 %, and 22 %, respectively. According to the current study's total water absorption assessment, using ultrafine CeO2 particles as supplemental cementitious materials (SCM) in concrete impeded the efficient flow of water (as well as potentially hazardous chemicals contained in water, such as sulfate and chloride).

3.8. Electrical resistivity

As noted in ACI 222R-01 [81], measuring the electrical resistivity of concrete has gained increasing importance as a method for assessing corrosion hazards associated with concrete structures. The movement of ions within the concrete matrix is demonstrated by electrical resistivity [82]. Furthermore, as concrete's permeability increases, ions may enter more easily and rapidly. In contrast, concrete with higher electrical resistance and lesser penetrability exhibits superior resistance to destructive ions, such as chloride [83,84]. Several variables influence concrete electrical resistance, including temperature, moisture content, pore solution composition, hydration level, and pore structure [84]. Fig. 14 shows the resistivity values at 28 and 90 days of age. The findings demonstrated that the electrical resistance of all RCA concrete mixes, including ultra-fine cerium dioxide, was more excellent than that of the RCA-UFCe0 mix. The resistance of RCA-UFCe0.5, RCA-UFCe1and

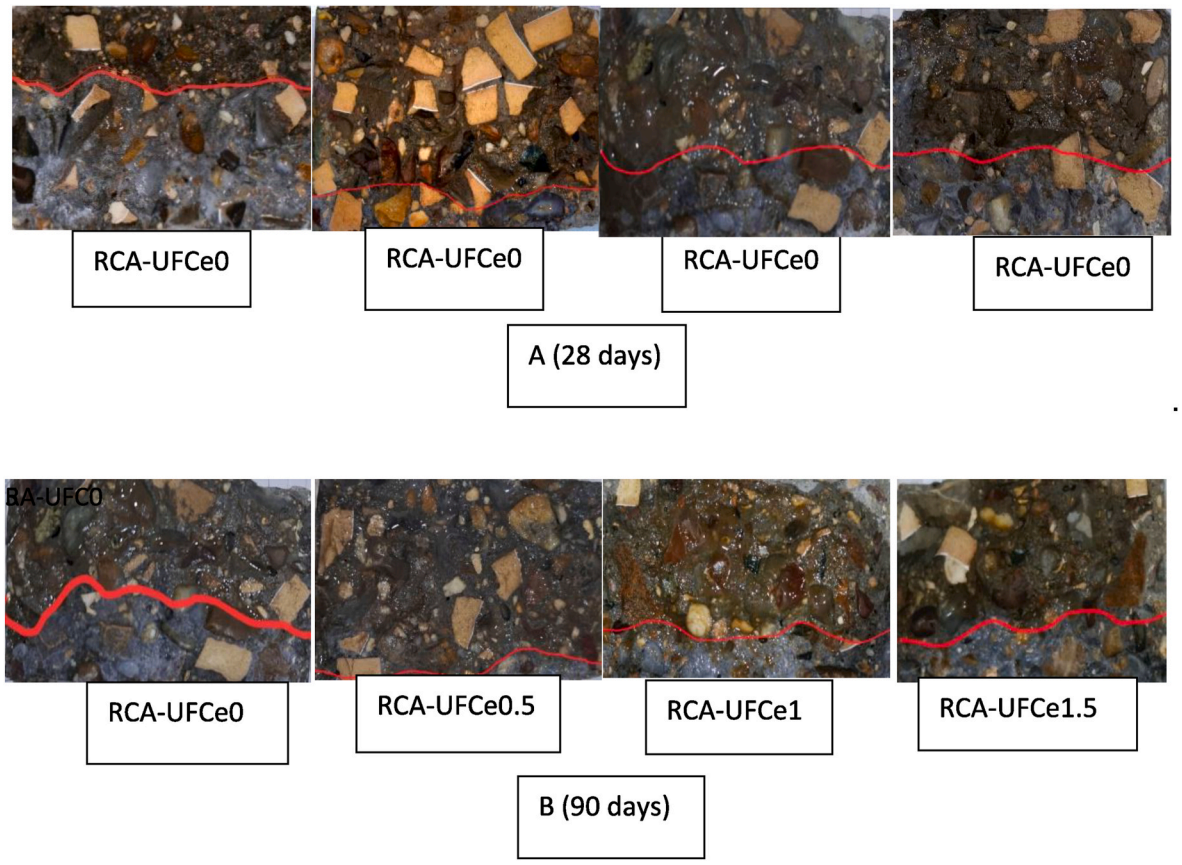

Fig. 15. RCA concrete mix depth of chloride penetration with and without UFCe at: A (28 days), B (90 days).

RCA-UFCe1.5 mixes at 28 days is 15.24,13.73 and 12.14 kΩ.cm respectively, which are higher than (11.9) of the RCA-UFCe0 mix by 28 %,15 %and 2 %and respectively. This indicates that 0.5 % was the highest beneficial level. Electrical resistivity increased with curing age in all RCA-UFCe mixes, consistent with the permeability and porosity results. The electrical resistivity of the RCA-UFCe0.5, RCA-UFCe1, and RCA-UFCe1.5 mixes at 90 days of age is 18.14, 15.61, and 14.27 kΩ cm, respectively, which are higher than (13.55) of the RCA-UFCe0 mix by 34 %,15 %and 5 % respectively. The higher electrical resistivity due to the inclusion of UFCe is due to its effects on the porosity, pore structure, and pore solutions of concrete. Hydration products such as Na^{+}, K^{+}, Ca^{2+}, and OH^{-} are present in the pore solution of RCA-UFCe0. These ions act as charge carriers. After adding UFCe to the RCA-UFCe0 mixture, these ions are adsorbed or deposited on the initial hydration (C–S–H and ettringite; AFt), allowing for decreased mobility of these ions which contributes to the creation of an electrical insulating layer around the cement grains [51]. The concentration of OH^{-} and Ca2+ ions decreases, resulting in the formation of a C–S–H gel, which will have a lower Ca/Si ratio. As a result, the electrical resistance increases when the improved microstructure is combined with the lower ion concentration in the pore solution [85]. In addition, as noted earlier about the effect of cerium on setting time, the inclusion of UFCe in the RCA concrete mixture resulted in a higher electrical resistivity than that in the RCA-UFCe0 mixture due to the lower free water in the concrete mixture caused by the higher water absorption of UFCe. These findings showed that, even though the cement content was decreased, the electrical resistivity was unaffected when CeO2-ultra fine-sized particles were used in place of cement. Every RCA mix containing UFCe has electrical resistivity readings higher than 13.6 kΩ cm. This is categorized as having "High" to "Very High" corrosion protection levels per ACI 222R-01 [81].

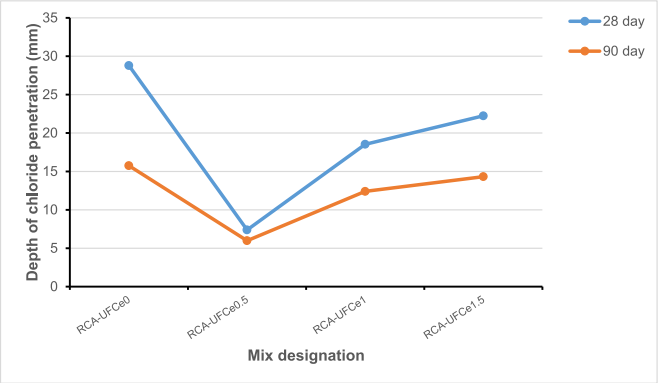

Fig. 16. RCA concrete mix chloride penetration depth value with and without UFCe at 28 and 90 days.

3.9. Depth of chloride ion penetration

A migration test was conducted at the ages of 28 and 90 days. A 0.1 N silver nitrate solution was applied to the specimen's recently fractured surfaces to gauge the extent of chloride ion penetration. The cross-section of the concrete specimens treated with AgNO3 solution to assess the level of penetration is shown in Fig. 15. The presence of silver chloride is why the surface of the concrete sample showed a lighter color. This white deposit indicates the amount of chloride penetration. On the other hand, the inside parts of the samples appeared darker due to the production of silver hydroxide. The depth of chloride ion penetration into RCA-UFCe concrete is shown in Fig. 16. Since the ultrafine CeO2 particles have excellent particle packing density in the

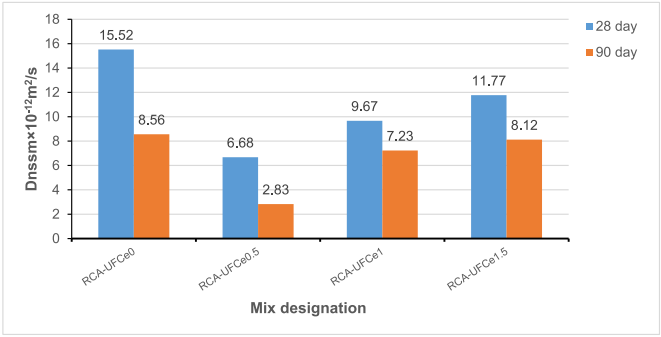

Fig. 17. RCA concrete mix chloride migration coefficient value with and without UFCe at 28 and 90 days.

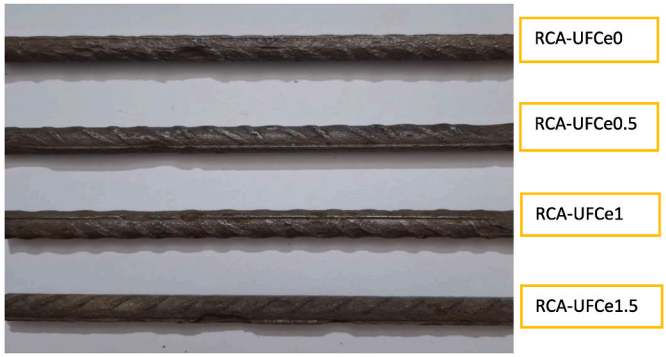

Fig. 18. Images of the steel rebars inserted into various RCA-UFCe concrete samples before sandblasting.

cementitious system, their addition leads to void filling and thus chloride permeability is reduced at both 28 and 90 days. Also, when UFCe is added to RCA concrete, it interacts with the calcium hydroxide and starts to build a larger quantity of calcium silicate hydrate gel network, which reduces the penetration of chloride [86]. Considering into account the findings from Fig. 16 regarding the penetration of chloride ions into RCA-UFCe both with and without UFCe, the depths of chloride ion penetration for the RCA-UFCe0.5, RCA-UFCe1and RCA-UFCe1.5 concretes (UFCe replacement levels of 0.5, 1and1.5respectively)at the age of 28 days were (7.38, 18.53and 22.24) mm, which was approximately 74.37 %,35.64 %and 22.75 % less than that of the RCA -UFCe0 mix, respectively, chloride penetration depth also decreases over time as a result of the ongoing hydration of the cement and the occlusion of the concrete's pore structure by CeO2 ultra-fine particles [87,88]. Where decreased to (5.98,12.4 and 14.32) mm at the age of 90 days, which was approximately,62 %,22 %and 7.44 % lower than that of the RCA-UFCe0 mix. The results demonstrated that the RCA concrete mix with 0.5 % UFCe exhibited the lowest penetration depth at both 28 and 90 days of curing. This finding aligns with the mechanical strength and electrical resistance results obtained at the same ages, which also showed the highest values at the 0.5 % replacement ratio. This suggests that the addition of effective CeO2-ultra fine-sized particles, which altered the pore structure of RCA concrete to a dense condition, had a definite positive impact on the durability of RCA concrete in terms of the resistance to chloride ion penetration when UFCe was used as a binder in place of PC, especially for longer curing ages. Chloride penetration is, therefore, quite challenging in this situation.

3.10. Non-steady-state diffusion coefficients of chloride ions (Dnssm)

The fast chloride migration coefficient test was used to evaluate RCA-UFCe concrete's ability to resist chloride ion penetration. The chloride migration coefficient of RCA-UFCe concrete mixes may thus be calculated for curing ages of 28 and 90 days using the chloride migration coefficient provided in Equation (3). The non-steady-state migration coefficients (Dnssm) for RCA-UFCe0 and modified RCA-UFCe concrete mixes at all selected ages are displayed in Fig. 17. At 28 days, the Dnssm of RCA containing UFCe are lower than that of RCA-UFCe0 (reference mix) by 57 %, 27 %%, and 6 % for RCA-UFCe0.5, RCA-UFCe1, and RCA-UFCe1.5 respectively, as shown in Fig. 17. UFCe, a finer particle size, fills the concrete skeleton, increasing its packing density and blocking permeable pores. It fills interstices between cement particles, promoting compactness and hindering chloride transport. Additionally, CeO2-ultra-fine particles encourage hydration due to the high surface area of the CeO_2 particles, which facilitates the nucleation of hydration products, resulting in a more uniform and compact microstructure for the cement matrix [89]. The fast chloride migration coefficient of RCA-UFC e concrete mixes exhibited an enormous change at 90 days compared to 28 days, which can be attributed to the continued development of the microstructure and the ongoing hydration reactions facilitated by the CeO_2 particles. As hydration progresses, the concrete matrix becomes denser, further reducing the pathways available for chloride ions to migrate.The chloride migration coefficient of RCA-UFCe0.5, RAC-UFCe1 and RCA-UFCe1.5, after 90 days fell by 57.63 %, 25.23 %, and 31.01 % respectively, compared to that at 28 days. The RCA-UFCe Concrete mix's microstructure densifies, particularly at later curing ages, as a result of the main cement components (C3S and β-C2S) continuously hydrating and releasing C–H. The CeO2-ultra fine-sized particles consume the free C–H released through cement hydration to form the hydrogel products CCeH, CceAH, and CceASH, which fill the pores of the concrete structure [51]. Therefore, voids are reduced, and the fine microstructure is improved in RCA concrete mixes containing ultra-fine cerium oxide. RCA concrete mixes with O.5 % UFC indicated the lowest Dnssm value at 28 and 90 days. This trend in improving resistance to chloride penetration in RCA concretes modified with CeO2-ultra fine-sized particles was consistent with the observations made from the electrical resistivity test and mechanical strength results as discussed above. The findings of the Dnssm test show that the use of CeO2-ultra fine-sized particles as a supplemental cementitious material (SCM) at concentrations up to 1.5 % inhibits the diffusion/migration of chloride ions into concrete. The principal contributors are the increased density of the microstructure and the existence of convoluted routes for chloride ions arising from the pozzolanic reaction of CeO2 ultra-fine particles. These may extend the lifespan of reinforced concrete buildings subjected to chloride exposure.

3.11. Evaluation of corrosion rate and mass loss of steel exposed to corrosive conditions

The passive protective film (PPF) is created spontaneously when reinforcing steel bars are implanted in concrete containing a high alkalinity of pore solution (pH 12–13). Soon after cement hydration begins, this film forms on its own accord [90]. When chloride ions infiltrate the concrete and reach the layer of concrete neighboring the reinforcing steel rebar this layer of protection surrounding the rebar is broken down and destroyed due to chloride ions and the surface of the steel becomes an anode electrode, which triggers an electrochemical reaction [91]. As a result of this reaction, the reinforcing steel corrodes, changing from its natural color to a black or red rust color, and developing pits on its surface [92]. After 26 days of subjecting to chloride solution and impress current, the RCA-UFCe concrete prisms are carefully broken to get out the rebar that is embedded in the RCA-UFCe concrete without damage, then the rebar is cleaned by using a sandblast machine and stiff metal brush out the rust as the showed in Fig. 18. The weights of the rebar are measured and recorded before casting and after sand blast shooting; Then, according to the American Society for Testing and Materials (ASTM G1) [93], a mass loss and corrosion rate test was conducted as shown in equations (5) and (6):

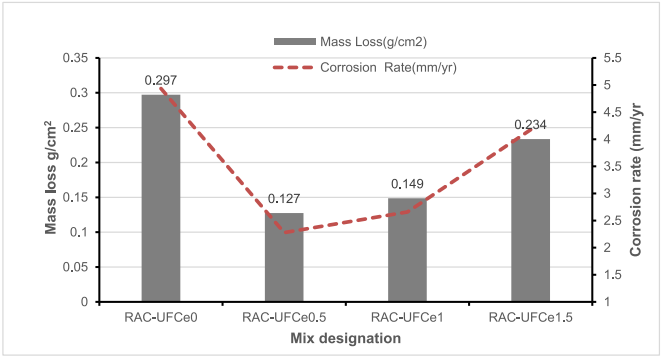

Fig. 19. Gravimetric mass loss and corrosion rate of RCA -UFCe concrete mixes with and without UFCe at 28 days of age.

$$\text{Mass Loss} = \frac{AMi - MF}{CA}(\text{g / cm2}) \tag{5}$$

$$\text{Corrosion Penetration Rate} = \frac{K \times W}{A \times T \times D}\ (\text{mm / yr}) \tag{6}$$

where A stands for exposed surface area (cm^2), T for exposure time (hours), D for alloy density (g/cm2), Mi for initial mass (g), Mf for final mass (g), and K for constant for unit needed (8.76*104).

Fig. 19 displays the mass loss and corrosion rate findings. It is evident that when UFCe is substituted for cement, the steel bar's gravimetric mass loss and corrosion rate reduce. The corrosion rate and weight loss for the mixes containing ultra-fine cerium dioxide, RCA-UFCe0.5, RCA-UFCe1, and RCA-UFCe1.5 are (2.278, 2.657, and 4.177) mm/yr and (0.127, 0.148 and 0.234) g/cm^2, are less than what is in the (RA-UFCe0) reference mix by (53.84 %,46.17 % and 15.73 %) and (57.23 %,49.83 % and 21.12 %) in that order. According to the findings, the RCA mix with 0.5 % ultra-fine cerium oxide exhibited the lowest gravimetric mass loss and corrosion rate, aligning with the mechanical strength, chloride migration, and electrical resistivity test for this research. The notable enhancement in corrosion resistance of RCA-UFCe concrete mixes incorporating cerium oxide is attributed to reduced permeability, likely resulting from the uniformity of the microstructure, the enhancement of the concrete's pore structure [94], and the increased formation of C–S–H, which collectively contribute to a denser matrix with superior strength and diminished permeability [95]. In addition, the liberation of cerium cations from the tiny cerium oxide particles, their migration to the metal surface, and their subsequent redeposition at the corrosion regions. In fact, the solubility of particles increases as their size decreases, resulting in the liberation of cerium cations. In addition, including cerium dioxide particles can enhance the corrosion resistance of metal alloys by cerium's intense attraction to oxygen, reducing oxygen levels in the active area [47]. The experimental investigations utilizing the Impressed Current Technique on the corrosion resistance of reinforcements in RA concrete with UFC additives demonstrated that the use of ultra-fine cerium oxide significantly enhances corrosion resistance. The gravimetric mass loss and the corrosion rate were the least in RA-UFCe containing UFC as compared to RA-UFCe without UFC which

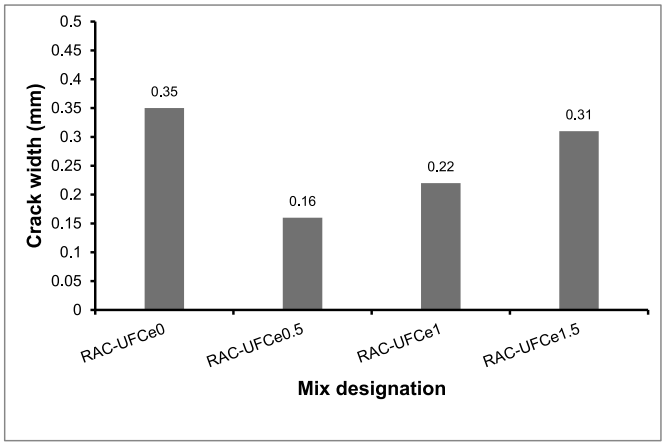

Fig. 21. The crack width for RCA -UFCe0 concrete specimen with and without UFCe.

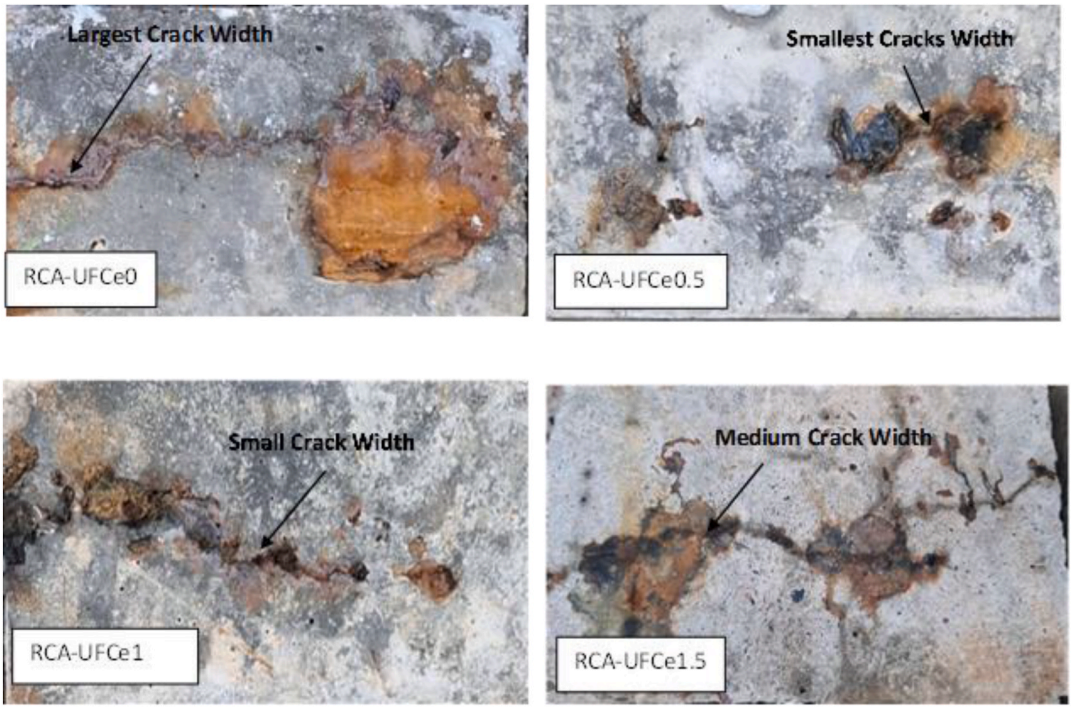

Fig. 20. The longitudinal, corrosion-induced splitting crack in the RCA-UFCe specimens with and without UFCe at 28 days of age.

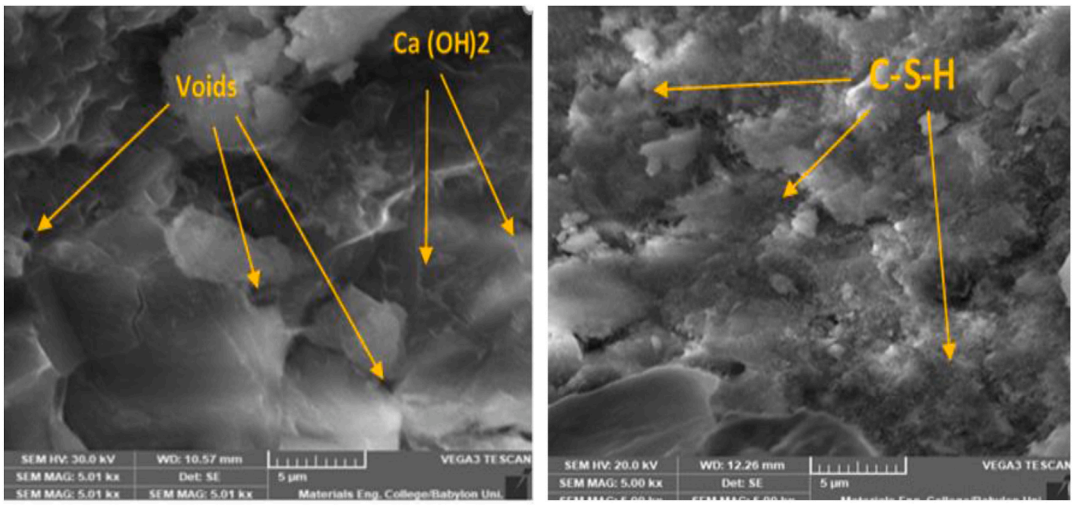

Fig. 22. SEM micrographs from the (a) control mixture RCA-UFCe0 at 5000 magnification power and (b) RCA -UFCe0.5 mixture containing 0.5 % UFCe at 5000 magnification power.

decreased the permeation of chloride ions to the rebar.

3.12. Cracks width

When reinforcing steel corrodes, more rust or corrosion products may build on its surface, creating internal pressure on the rebar's surrounding concrete. Cracks may appear along the concrete's face parallel to the reinforcing steel bar as a result of this increase in internal pressure [96]. The corrosion of the steel rod within the RCA concrete resulted in the formation of cracks on the concrete specimen's surface, parallel with the steel rod, as seen in Fig. 20. The crack width was measured using a microcrack meter. Fig. 21 shows the crack width for RCA-UFCe0 concrete mix and modified RCA-UFCe concrete mixes. The results of measuring the crack width of the concrete containing UFCe showed a much smaller crack width than that in the reference mixture. The smallest crack width measurement was in the RCA-UFCe mix containing 0.5 % cerium dioxide, which was 64.44 % less than the crack width in the reference sample. This is due to the smaller weight loss and lower corrosion rate of the RA mixture containing 0.5 % ultrafine cerium oxide, attributable to its filling capacity and decreased ion penetration due to enhanced pozzolanic reactions of UFCe [84,97]. According to certain studies, tiny particles provide a denser structure and increased discrete voids in concrete which will therefore reduce the corrosion rate and crack width [98].

3.13. Microstructural analysis

SEM analysis was conducted on sample pieces with the highest mechanical strength at 28 days of age (RCA-UFCe0.5) and control specimens (RCA-UFCe0). Fig. 22 displays the SEM images of mixes RCA-UFCe0 and RCA-UFCe0.5 at a magnification power of 5000×, represented by images(a and b), respectively. SEM images of RA-UFCe0 show a poor morphology structure as a result of the existence of enlarged voids, and porosity. This results from the RCA-UFCe0 mix's decreased hydration, which is insufficient to fill the specimen's pores. The scanning electron microscope (SEM) image of the RCA-UFCe0.5 mix revealed the presence of a combination of hydration products, predominantly consisting of a substantial amount of C–S–H gel. This gel plays a crucial role in connecting cement particles and forming a robust and compact structure, leading to a significant reduction in the porosity of the RCA-UFCe0.5 mix. This reflects the influence of UFCe on the chemical and physical properties of RCA concrete. Chemically, the nucleation and pozzolanic interaction with free portlandite promote cement hydration and produce further cementitious materials including CCeH, CCeAH, and CCeASH hydrated gel products [16,66]. According to its physical properties, UFCe is approximately 97 times smaller than cement particles. It can occupy the empty spaces in the cement paste and enhance the overall density of concrete [45]. Consequently, the RCA-UFCe0.5 specimen shows a lower pore content and a more compact microstructure. This observation aligns with the mechanical testing results.

4. Conclusions

The present study sought to examine the impact of ultrafine cerium dioxide particles on enhancing the physical, mechanical, corrosion resistance, and chloride permeability properties of recycled ceramic aggregate concrete) RCA). The ultrafine cerium dioxide particles utilized in our study were synthesized by a grinding technique employing micronized cerium dioxide (D50 = 20 μm) as raw material. A laser particle analyzer (Malvern MS3000) was used to examine the milled cerium oxide's particle size, and it was determined that the particles' average size was around 350 nm. The ultrafine cerium dioxide particles embedded in the RA concrete reduced the pore size Ultrafine cerium dioxide particles incorporated into corrosion-resistant RCA concrete resulted in reduced pore size resulting in filling capacity and decreased ion penetration due to greater pozzolanic interactions of UFCe. The study yields the following conclusions.

1. Augmenting the substitution ratio of ordinary Portland cement with ultra-fine cerium dioxide diminishes the slump value and impairs the workability of the RCA concrete. The most significant reduction in the slump value (14 %) was observed at 1.5 % UFC. Furthermore, the initial and final setting times for concrete diminished as the fraction of PC replaced by UFCe increased. The minimum initial and final setting periods were observed at a 1.5 % replacement rate, 14 and 10 min shorter than those of 100 % cement paste.
2. Compared to all RCA concrete mixes containing ultrafine cerium oxide, the RCA-UFCe0.5 mix's compressive and tensile strengths showed higher values for up to 90 days. The tensile and compressive strengths rose by 29 % and 7 % after 90 days and by 33 % and 23 % at 28 days. Although the compressive and tensile strengths dropped when the UFCe percentage was raised from 0.50 to 1.5 %, they were still higher than the reference mix's values.

3. RCA concrete with ultra-fine cerium dioxide exhibited reduced percentages of permeable pores and total water absorption compared to the reference mixture (RCA-UFCe0). The lowest water absorption and permeability at 28 and 90 days were obtained with the addition of 0.5 % ultrafine cerium oxide; these were 26 % and 28 % lower than those of the control mixture at 28 days, and 42 % and 45 % less than those of the reference specimen at 90 days.
4. The analysis of the microstructure of (RCA-UFCe0.5) and control specimens (RCA-UFCe0) using SEM demonstrated that the incorporation of ultra-fine cerium dioxide (UFCe) markedly improves the microstructure of RCA concrete.
5. The addition of ultra-fine cerium oxide significantly improves the corrosion resistance of RCA concrete mixes. The corrosion rate, weight loss, and crack width were reduced considerably in all mixes containing ultrafine cerium dioxide compared to the reference mix. The mix containing 0.5 % ultrafine cerium oxide showed the lowest corrosion rate, weight loss, and crack width, 54 %, 58 %, and 64.44 % lower than the reference mix.
6. This paper concludes that ultrafine cerium dioxide-based concrete is especially appropriate for use in chloride environments owing to its corrosion-resistant qualities. Moreover, including ultrafine cerium dioxide particles in the cement matrix enhances the system's durability and facilitates the production of C–S–H gel. This primary hydration product regulates the mechanical properties of concrete.

Data availability statement

The authors confirm that the data supporting the findings of this study are available on request.

Funding information

This research did not receive any funding.

Declaration of competing interest

The authors declare that they have no known competing financial interests or personal relationships that could have appeared to influence the work reported in this paper.

References

[1] Tobeia SB, Assi NS, Abbas NS. Mechanical properties prediction of normal and high strength geopolymer concrete. Eng Technol J 2021;39:1781–8.
[2] Wan S, Li S, Chen Z, Tang Y. An ultrasonic-AI hybrid approach for predicting void defects in concrete-filled steel tubes via enhanced XGBoost with Bayesian optimization. Case Stud Constr Mater 2025:e04359.
[3] Sayhood EK, Al-Hamdani MAE, Sahan JK. Effect of recycled aggregate on behavior of tied and spiral reinforced fibrous circular short columns. Eng Technol J 2021;39:1945–52.
[4] Batikha M, Ali STM, Rostami A, Kurtayev M. Using recycled coarse aggregate and ceramic waste to produce sustainable economic concrete. Int J Sustain Eng 2021;14:785–99.
[5] Kubba HZ, Nasr MS, Al-Abdaly NM, Dhahir MK, Najim WN. Influence of incinerated and non-incinerated waste paper on properties of cement mortar. IOP Conf Ser Mater Sci Eng 2020. https://doi.org/10.1088/1757-899X/671/1/012113.
[6] Kajaste R, Hurme M. Cement industry greenhouse gas emissions–management options and abatement cost. J Clean Prod 2016;112:4041–52.
[7] Environment UN, Scrivener KL, John VM, Gartner EM. Eco-efficient cements: potential economically viable solutions for a low-CO2 cement-based materials industry. Cement Concr Res 2018;114:2–26.
[8] Paul SC, Faruky SAU, Babafemi AJ, Miah MJ. Eco-friendly concrete with waste ceramic tile as coarse aggregate: mechanical strength, durability, and microstructural properties. Asian J. Civ. Eng. 2023;24:3363–73. https://doi.org/10.1007/s42107-023-00718-x.
[9] Turki SK, Ibrahim SI, Almaamori MHD. The impact of incorporating waste materials on the mechanical and physical characteristics of tile adhesive materials. Open Eng 2024;14:20220580.
[10] Azeez AT, Hassan MS, Atiyah AA. Evaluation of the performance of steel slag and waste glass as a cement replacement. Eng Technol J 2023;41:1567–77. https://doi.org/10.30684/etj.2023.143602.1597.
[11] Hashim AA, Azeez NS, Naje AS, Al-Zubaidi HAM. Eco friendly enhancement of self-compacting concrete mechanical properties using metakaolin and nanosilica. J. Green Eng. 2021;11:1748–66.
[12] Chen Z, Yu J, Nong Y, Yang Y, Zhang H, Tang Y. Beyond time: enhancing corrosion resistance of geopolymer concrete and BFRP bars in seawater. Compos Struct 2023;322:117439.
[13] Tang Y, Feng W, Chen Z, Mai J, Zheng J, Yang Y. Behaviour of steel-reinforced recycled aggregate concrete-filled GFRP tubular short columns under eccentric axial compression. Thin-Walled Struct 2024;199:111818.
[14] Hasan ZA, Abed MK, Nasr MS. Studying the mechanical properties of mortar containing different waste materials as a partial replacement for aggregate. Int. Rev. Civ. Eng. 2019;10:155. https://doi.org/10.15866/irece.v10i3.16943.
[15] Baraldi L, by Acimac M-MES. World production and consumption of ceramic tiles. Oceania 2016;56. 0–4.
[16] Hashim AA, Anaee R, Nasr MS. Improving the mechanical, corrosion resistance, microstructural and environmental performance of recycled aggregate concrete using ceramic waste powder as an alternative to cement. Ceramics 2025;8:11.
[17] Martínez-Barrera G, Ávila-Córdoba LI, Martínez-López M, Herrera-Sosa ES, Vigueras-Santiago E, Barrera-Díaz CE, Ureña-Nuñez F, González R. Gamma radiation as a recycling tool for waste materials used in concrete, Evol. Ioniz. Radiat. Res. Rijeka Croat. Tech. 2015:259–79.
[18] Gharibi H, Mostofinejad D, Bahmani H, Hadadzadeh H. Improving thermal and mechanical properties of concrete by using ceramic electrical insulator waste as aggregates. Constr Build Mater 2022;338:127647.
[19] Suzuki M, Seddik Meddah M, Sato R. Use of porous ceramic waste aggregates for internal curing of high-performance concrete. Cement Concr Res 2009;39:373–81. https://doi.org/10.1016/j.cemconres.2009.01.007.
[20] García-González J, Rodríguez-Robles D, Juan-Valdés A, Morán-del Pozo JM, Guerra-Romero MI. Ceramic ware waste as coarse aggregate for structural concrete production. Environ Technol 2015;36:3050–9.
[21] Torkittikul P, Chaipanich A. Utilization of ceramic waste as fine aggregate within Portland cement and fly ash concretes. Cem Concr Compos 2010;32:440–9.
[22] Nepomuceno MCS, Isidoro RAS, Catarino JPG. Mechanical performance evaluation of concrete made with recycled ceramic coarse aggregates from industrial brick waste. Constr Build Mater 2018;165:284–94.
[23] Sekar T, Ganesan N, Nampoothiri NVN. Studies on strength characteristics on utilization of waste materials as coarse aggregate in concrete. Int J Eng Sci Technol 2011;3:5436–40.
[24] Reddy MV. Investigations on stone dust and ceramic scrap as aggregate replacement in concrete. Int J Civ Struct Eng 2010;1:661–6.
[25] Zeng Z, Wan C. Experimental research on basic mechanical properties of recycled ceramic concrete. In: Proc. Shanghai Int. Conf. Technol. Archit. Struct. Shanghai, China; 2009. p. 1–3.
[26] Cabral AEB, Schalch V, Dal Molin DCC, Ribeiro JLD. Mechanical properties modeling of recycled aggregate concrete. Constr Build Mater 2010;24:421–30.
[27] De Brito J, Pereira AS, Correia JR. Mechanical behaviour of non-structural concrete made with recycled ceramic aggregates. Cem Concr Compos 2005;27:429–33.
[28] Zheng C, Lou C, Du G, Li X, Liu Z, Li L. Mechanical properties of recycled concrete with demolished waste concrete aggregate and clay brick aggregate. Results Phys 2018;9:1317–22.
[29] Gomes M, de Brito J. Structural concrete with incorporation of coarse recycled concrete and ceramic aggregates: durability performance. Mater Struct 2009;42:663–75.
[30] Anderson DJ, Smith ST, Au FTK. Mechanical properties of concrete utilising waste ceramic as coarse aggregate. Constr Build Mater 2016;117:20–8.
[31] Hashim AA, Anaee R, Nasr MS. Enhancing the sustainability, mechanical and durability properties of recycled aggregate concrete using calcium-rich waste glass powder as a supplementary cementitious material: an experimental study and environmental assessment. Sustain. Chem. Pharm. 2025;44:101985. https://doi.org/10.1016/j.scp.2025.101985.
[32] Gao C, Huang L, Yan L, Jin R, Chen H. Mechanical properties of recycled aggregate concrete modified by nano-particles. Constr Build Mater 2020;241:118030.
[33] Zhan BJ, Xuan DX, Zeng W, Poon CS. Carbonation treatment of recycled concrete aggregate: effect on transport properties and steel corrosion of recycled aggregate concrete. Cem Concr Compos 2019;104:103360.
[34] Zeng W, Zhao Y, Poon CS, Feng Z, Lu Z, Shah SP. Using microbial carbonate precipitation to improve the properties of recycled aggregate. Constr Build Mater 2019;228:116743.
[35] Hashim AA, Owaid HM. A review of workability and mechanical behavior of Self-compacting construction composites incorporating nanomaterials. J. Univ. Babylon Eng. Sci. 2024;32:119–31.
[36] Hashim AA, kazem Rodhan Z, Abbas SJ. Fresh and hardened properties of self-compacting high performance concrete containing nano-metakaolin as a partial replacement. In: IOP Conf. Ser. Mater. Sci. Eng. IOP Publishing; 2020, 22036.
[37] Hashim AA, Azeez NS, Naji AS. Eco friendly enhancement of self- compacting concrete mechanical properties using metakaolin and nanosilica. J. Green Eng. 2021;11.
[38] H. AbdullahDeposition of CeO2/TCP thin film on stainless steel 316 L by RF sputtering, Al-Ghaban A, Anaee R. Deposition of CeO2/TCP thin film on stainless steel 316 L by RF sputtering. Eng Technol J 2021;39:625–31.
[39] Abdulaah HA, Al-Ghaban AM, Anaee RA, Khadom AA, Kadhim MM. Cerium-tricalcium phosphate coating for 316L stainless steel in simulated human fluid: experimental, biological, theoretical, and electrochemical investigations. J Electrochem Sci Eng 2023;13:115–26.

[40] Tan P, Shu X, Wen M, Li L, Lu Y, Lu X, Chen S, Dong F. Characteristics of cerium doped aluminosilicate glass as simulated radioactive waste forms: effect on structures and properties. Prog Nucl Energy 2022;150:104299.
[41] Taniguchi MM, da Silva E, da Silva MAT, Herculano LS, Muniz RF, Sandrini M, Belançon MP. The role of Ce3+/Ce4+ in the spectroscopic properties of cerium oxide doped zinc-tellurite glasses prepared under air. J Non-Cryst Solids 2020;547:120307.
[42] Sandrini M, Gemelli JC, Gibin MS, Zanuto VS, Muniz RF, de Vicente FS, Belançon MP. Synthesis and properties of Cerium-doped organic/silica xerogels: a potential UV filter for photovoltaic panels. J Non-Cryst Solids 2023;600:122033.
[43] Jayakumar G, Irudayaraj AA, Raj AD, Sundaram SJ, Kaviyarasu K, Jayakumar G, Irudayaraj AA, Raj AD, Sundaram SJ, Kaviyarasu K. Electrical and magnetic properties of nanostructured Ni doped CeO2 for optoelectronic applications. J Phys Chem Solid 2022;160:110369.
[44] Juthapakdeeprasert J, Gavalda Diaz O, Lerdprom W, De Sousa Meneses D, Jayaseelan DD, Lee WE. Reactions and emissivity of cerium oxide with phosphate binder coating on basic refractory brick. Int J Appl Ceram Technol 2020;17:668–76.
[45] Majdi MR, Danaee I, Afghahi SSS. Preparation and anti-corrosive properties of cerium oxide conversion coatings on steel X52. Mater Res 2017;20:445–51.
[46] Creus J, Brezault F, Rebere C, Gadouleau M. Synthesis and characterisation of thin cerium oxide coatings elaborated by cathodic electrolytic deposition on steel substrate. Surf Coating Technol 2006;200:4636–45.
[47] Harb SV, Trentin A, de Souza TAC, Magnani M, Pulcinelli SH, Santilli CV, Hammer P. Effective corrosion protection by eco-friendly self-healing PMMA-cerium oxide coatings. Chem Eng J 2020;383:123219.
[48] Liu X, Wu Z, Lyu Y, Li T, Yang H, Liu Y, Liu R, Xie X, Lyu K, Shah SP. Corrosion resistance of CeO2-GO/epoxy nanocomposite coating in simulated seawater and concrete pore solutions. Polymers 2023;15:2602.
[49] Montemor MF, Pinto R, Ferreira MGS. Chemical composition and corrosion protection of silane films modified with CeO2 nanoparticles. Electrochim Acta 2009;54:5179–89.
[50] Motny RM, Phongikaroon S. Effects of cerium concentration and solvent on physical and chemical characterization of rapid setting cement. Nucl Technol 2019;205:671–83.
[51] Ibrahim SM, Heikal M, Mohamed OA. Performance of CeO2-nanoparticles on the mechanical and photocatalytic properties of composite cement. J Build Eng 2023;68:106162.
[52] A.S. for T. and Materials. ASTM C150/C150M standard specification for Portland cement. 2015.
[53] Q.S. No. 45. Aggregate from natural sources for concrete and construction, 11. Baghdad, Iraq: Central Organization for Standardization & Quality Control (COSQC); 1984n.d..
[54] ASTM C 494/C 494M – 08. Standard specification for chemical admixtures for concrete. ASTM; 2008. n.d.
[55] ASTM C143-03, ASTM C 143/C 143M – 03 Standard Test Method for Slump of Hydraulic-Cement Concrete. Annu Book ASTM Stand 2003:1–4.
[56] ASTMC191-08. Standard test methods for time of setting of hydraulic cement by Vicat needle. ASTM Int. 2009;4(C):1–8 [Online]. Available: www.astm.org. n.d..
[57] BS 1881-116, –testing concrete — Part 116: method for determination of compressive strength of concrete cubes. British Standard, December 2003 [n.d.].
[58] No TitleASTM-C496. Standard test method for splitting tensile strength of cylindrical concrete specimens. American Society for Testing and Materials.; 2002. n.d.
[59] ASTM C642, A. Standard test method for density, absorption, and voids in hardened concrete. ASTM, ASTM Int.; 2013. n.d.
[60] ASTM C1876-19. Standard test method for bulk electrical resistivity or bulk conductivity of concrete. ASTM; 2023. n.d.
[61] Gopalakrishnan R, Nithiyanantham S. Microstructural, mechanical, and electrical properties of copper slag admixtured cement mortar. J Build Eng 2020;31:101375. https://doi.org/10.1016/j.jobe.2020.101375.
[62] NT Build 492. Chloride migration coefficient from non-steady-state migration experiments key. 1999.
[63] Feng W, Tarakbay A, Memon SA, Tang W, Cui H. Methods of accelerating chloride-induced corrosion in steel-reinforced concrete: a comparative review. Constr Build Mater 2021;289:123165.
[64] Vandhiyan R, Pillai EB. Influence of nano silica addition on the behavior of concrete and its impact on corrosion resistance. J Comput Theor Nanosci 2018;15:530–6.
[65] Alwash SS, AL-Ameeri AS, Mattar SG. Assessing the effect of corrosion on optimised low carbon concrete. Mater Today Proc 2023.
[66] Li L, Xuan D, Sojobi AO, Liu S, Chu SH, Poon CS. Development of nano-silica treatment methods to enhance recycled aggregate concrete. Cem Concr Compos 2021;118:103963.
[67] Bourchy A, Yamagata ALF, Smith GL, Sevigny GJ, Seiner BN, Saslow SA. Cerium oxide impact on fresh and hardened properties of cementitious materials. Cem Concr Compos 2023;138:104976.
[68] Bin Muhit I, Sheikh SA, Zaman MF, Ullah MS. Effects of multiple supplementary cementitious materials on workability and strength of lightweight aggregate concrete, Jordan. J Civ Eng 2018;12:109–24.
[69] Mounanga P, Khokhar MIA, El Hachem R, Loukili A. Improvement of the early-age reactivity of fly ash and blast furnace slag cementitious systems using limestone filler. Mater Struct 2011;44:437–53.
[70] Meng T, Wei H, Ying K, Wang M. Analysis of the effect of nano-SiO2 and waterproofing agent on the water transportation process in mortar using NMR. Appl Sci 2020;10:7867.
[71] Ibrahim SM, Heikal M, Abdelwahab NR, Mohamed OA. Fabricated CeO2/ZrO2 nanocomposite to improve thermal resistance, mechanical characteristics, microstructure and gamma radiation shielding of OPC composite cement pastes. Constr Build Mater 2023;392:131971. https://doi.org/10.1016/j.conbuildmat.2023.131971.
[72] Nasr MS, Ali IM, Hussein AM, Shubbar AA, Kareem QT, AbdulAmeer AT. Utilization of locally produced waste in the production of sustainable mortar. Case Stud Constr Mater 2020;13:e00464. https://doi.org/10.1016/j.cscm.2020.e00464.
[73] Oltulu M, Şahin R. Pore structure analysis of hardened cement mortars containing silica fume and different nano-powders. Constr Build Mater 2014;53:658–64.
[74] Tariq S, Scott AN, Mackechnie JR, Shah V. Durability of high volume glass powder self-compacting concrete. Appl Sci 2020;10:8058.
[75] Lian C, Zhuge Y, Beecham S. The relationship between porosity and strength for porous concrete. Constr Build Mater 2011;25:4294–8.
[76] Wu Z, Shi C, Khayat KH, Wan S. Effects of different nanomaterials on hardening and performance of ultra-high strength concrete (UHSC). Cem Concr Compos 2016;70:24–34.
[77] Singh G, Siddique R. Effect of iron slag as partial replacement of fine aggregates on the durability characteristics of self-compacting concrete. Constr Build Mater 2016;128:88–95.
[78] Mehta PK, Monteiro PJM. Concrete: microstructure, properties, and materials. McGraw-Hill Education; 2014.
[79] Mohseni E, Miyandehi BM, Yang J, Yazdi MA. Single and combined effects of nano-SiO2, nano-Al2O3 and nano-TiO2 on the mechanical, rheological and durability properties of self-compacting mortar containing fly ash. Constr Build Mater 2015;84:331–40.
[80] Heikal M, Zaki MEA, Ibrahim SM. Characterization, hydration, durability of nano-Fe2O3-composite cements subjected to sulphates and chlorides media. Constr Build Mater 2021;269:121310.
[81] ACI 222R-01 protection of metals in concrete against corrosion. Farmington Hills: American Concrete Institute; 2009 [n.d.].
[82] Pilvar A, Ramezanianpour AA, Rajaie H, Karein SMM. Practical evaluation of rapid tests for assessing the chloride resistance of concretes containing silica fume. Comput. Concr. An Int. J. 2016;18:793–806.
[83] Delnavaz M, Sahraei A, Delnavaz A, Farokhzad R, Amiri S, Bozorgmehrnia S. Production of concrete using reclaimed water from a ready-mix concrete batching plant: life cycle assessment (LCA), mechanical and durability properties. J Build Eng 2022;45:103560.
[84] Karein SMM, Ramezanianpour AA, Ebadi T, Isapour S, Karakouzian M. A new approach for application of silica fume in concrete: wet granulation. Constr Build Mater 2017;157:573–81.
[85] Li W, Li X, Chen SJ, Liu YM, Duan WH, Shah SP. Effects of graphene oxide on early-age hydration and electrical resistivity of Portland cement paste. Constr Build Mater 2017;136:506–14.
[86] Nandhini K, Ponmalar V. Investigation on nano-silica blended cementitious systems on the workability and durability performance of self-compacting concrete. Mater. Express. 2020;10:10–20.
[87] Chithra S, Kumar SRRS, Chinnaraju K. The effect of Colloidal Nano-silica on workability, mechanical and durability properties of High Performance Concrete with Copper slag as partial fine aggregate. Constr Build Mater 2016;113:794–804.
[88] Nandhini K, Ponmalar V. Effect of blending micro and nano silica on the mechanical and durability properties of self-compacting concrete. Silicon 2021;13:687–95.
[89] Safiuddin M, Gonzalez M, Cao J, Tighe SL. State-of-the-art report on use of nano-materials in concrete. Int J Pavement Eng 2014;15:940–9.
[90] Ghods P, Isgor OB, McRae G, Miller T. The effect of concrete pore solution composition on the quality of passive oxide films on black steel reinforcement. Cem Concr Compos 2009;31:2–11.
[91] Ghoddousi P, Haghtalab M, Shirzadi Javid AA. Experimental and numerical investigation of repair dimensions effect on macro-cell corrosion induced by concrete slabs patch repair. Int J Civ Eng 2021;19:1091–110.
[92] Hameed A, Afzal MFUD, Javed A, Rasool AM, Qureshi MU, Mehrabi AB, Ashraf I. Behavior and performance of reinforced concrete columns subjected to accelerated corrosion. Metals 2023;13:930.
[93] A. G1. Standard practice for preparing, cleaning, and evaluation corrosion test specimens. 2003. n.d.
[94] Nejad FM, Tolouei M, Nazari H, Naderan A. Effects of calcium carbonate nanoparticles and fly ash on mechanical and permeability properties of concrete. Adv. Civ. Eng. Mater. 2018;7:651–68.
[95] Uthaman S, George RP, Vishwakarma V, Harilal M, Philip J. Enhanced seawater corrosion resistance of reinforcement in nanophase modified fly ash concrete. Constr Build Mater 2019;221:232–43.
[96] Berrocal CG, Löfgren I, Lundgren K, Tang L. Corrosion initiation in cracked fibre reinforced concrete: influence of crack width, fibre type and loading conditions. Corros Sci 2015;98:128–39.
[97] Said AM, Zeidan MS, Bassuoni MT, Tian Y. Properties of concrete incorporating nano-silica. Constr Build Mater 2012;36:838–44.
[98] Eskandari-Naddaf H, Ziaei-Nia A. Simultaneous effect of nano and micro silica on corrosion behaviour of reinforcement in concrete containing cement strength grade of C-525. Procedia Manuf 2018;22:399–405.